Canadian Mineralogist
Vol. 29, pp. 741-754 (1991)

UNIVARIANT MIXED-VOLATILE REACTIONS: PRESSURE–TEMPERATURE PHASE DIAGRAMS AND REACTION ISOGRADS

DUGALD M. CARMICHAEL
Department of Geological Sciences, Queen's University, Kingston, Ontario K7L 3N6

ABSTRACT

For any isobaric invariant point on a fully expanded temperature *versus* mol fraction (T–X) phase diagram, there is a pair of phase assemblages whose stability fields span the largest divariant sectors on the low-T and high-T sides of the point and do not overlap along the T axis. The two assemblages have no solid phases in common, but together they include all the phases of the isobarically invariant assemblage. The closed-system reaction that relates these two assemblages produces a fluid phase of isobarically invariant composition, and it can be mass-balanced algebraically without prior knowledge of the stable T–X topology, thus identifying the low-T and high-T phase assemblages in a simple and direct manner. These considerations justify and facilitate labeling of reactant and product assemblages on the polybaric P–T trace of any isobaric invariant point. In turn, such labeling facilitates direct chemographic expansion of H_2O–CO_2 or other mixed-volatile equilibria in P–T projection, bypassing the usual first step of constructing a complete set of stable T–X diagrams in the P range of interest. The resulting P–T phase diagrams are convenient in the determination and display of the P–T stability fields of silicate–carbonate mineral assemblages. Such diagrams also serve to identify critical subassemblages that are necessary and sufficient for rigorous mapping of isograds based on univariant mixed-volatile reactions and bathograds based on invariant mixed-volatile reactions.

Keywords: bathograd, buffering, chemography, infiltration, phase equilibria, siliceous marble, Italy, Japan, Switzerland.

SOMMAIRE

Pour chaque point isobariquement invariant d'un diagramme de phases T–X complet, donc exprimé en fonction de température et de fraction molaire, il y a une paire d'assemblages dont les champs de stabilité couvrent les secteurs bivariants les plus larges des deux côtés du point, soit vers une température plus faible et plus élevée; ces champs de stabilité s'excluent mutuellement le long de l'axe T. Ces deux assemblages ne possèdent aucune phase solide en commun, mais ensemble ils contiennent toutes les phases de l'assemblage isobariquement invariant. La réaction en système fermé qui lie ces deux assemblages produit une phase fluide de composition isobariquement invariante, qui peut être utilisée pour balancer la réaction sans connaissances préalables de la topologie T–X stable. Il est donc possible d'identifier les assemblages stables à températures faible et élevée de façon simple et directe. Ces considérations justifient et facilitent l'étiquettage des assemblages de réactifs et de produits sur un tracé polybarique P–T de n'importe quel point isobariquement invariant. De plus, un tel exercise facilite l'expansion chimiographique directe des équilibres impliquant H_2O et CO_2, ou autres équilibres impliquant un mélange de composants volatils, sans les constructions préliminaires de séries complètes de diagrammes T–X pour l'intervalle de pression en question. Les diagrammes P–T qui en résultent sont très utiles pour la détermination et la représentation des champs de stabilité P–T des assemblages impliquant silicates et carbonates. De tels diagrammes servent aussi à définir de façon rigoureuse les sous-assemblages critiques nécessaires et suffisants pour la cartographie rigoureuse d'isogrades fondés sur les réactions univariantes à phase volatile mixte et de bathogrades fondés sur les réactions invariantes à phase volatile mixte.

(Traduit par la Rédaction)

Mots-clés: bathograde, tamponage, chimiographie, infiltration, équilibre de phases, marbre siliceux, Italie, Japon, Suisse.

INTRODUCTION

Following its invention and elucidation by Greenwood (1962, 1967), the type of isobaric phase diagram on which temperature is plotted against the mol fraction of one of the molecular species in a "mixed-volatile" fluid phase has been widely applied in petrological studies. Typically, such "T–X" phase diagrams display equilibrium curves for several isobarically univariant reactions. These curves may intersect at one or more isobaric invariant points, each of which represents the intersection of a truly univariant P–T curve with the isobaric plane of the diagram.

Greenwood (1967) postulated that isobarically univariant reactions would tend to act as buffers of fluid composition during prograde metamorphism, and this was confirmed in the field by Trommsdorff (1972). Skippen (1974) pointed out

the importance of isobaric invariant points for geothermometry, and tabulated pairs of silicate–carbonate mineral assemblages, of which field occurrences could be used to "bracket" such points with respect to temperature. Greenwood (1975) developed a theoretical model of prograde metamorphism in silicate–carbonate rocks whereby the most abrupt changes in metamorphic mineralogy, which would be most readily mappable as isograds, are predicted to take place at isobaric invariant points, to which the composition of the fluid phase tends to be driven by prograde buffering. Such isograds were soon identified in the field (Trommsdorff & Evans 1977a, Rice 1977a, b, Suzuki 1977). However, to my knowledge, no such isograd has been mapped as rigorously as mineral-assemblage data might permit.

Several authors have projected the polybaric trace of one or more isobaric invariant points onto the P–T plane (Eugster & Wones 1962, Puhan & Hoffer 1973, Winkler 1974, Greenwood 1975, Skippen & Carmichael 1977, Trommsdorff & Evans 1977b, Ellis & Wyllie 1979, Erdmer 1981, Franz & Spear 1983), thus generating a diagram that displays one or more univariant P–T curves for mixed-volatile equilibria. Greenwood (1975) outlined a method of mass-balancing an isobarically invariant reaction (by linear combination of any two of the isobarically univariant reactions so as to produce fluid of isobarically invariant composition), but he stopped short of labeling the low-T (reactant) and high-T (product) assemblages on the corresponding univariant P–T curves. To my knowledge, the P–T curve for the simplest of all univariant mixed-volatile reactions, *brucite + magnesite = periclase + fluid*, is the only one to date that has been correctly labeled with reactants and products (Ellis & Wyllie 1979, Thompson 1983). *Note added in proof:* The chemography of univariant mixed-volatile equilibria has been investigated independently by Baker *et al.* (1991) and by Connolly & Trommsdorff (1991).

This paper explores some consequences of the fact that the polybaric P–T trace of any isobaric invariant point represents a unique "closed-system" reaction whose coefficients vary only with either P or T. Reactions in the system CaO–MgO–SiO_2–H_2O–CO_2 (CMSH–CO_2) will be used for illustration, but the chemographic principles to be discussed apply to any mixed-volatile system.

THE T–$X(CO_2)$ DIAGRAM

In Figure 1, isobaric univariant curves for five stable reactions radiate from an isobaric invariant point, at which the six-phase assemblage *tremolite – talc – quartz – calcite – dolomite – fluid* is stable. Although these reactions have slightly variable mass-balance coefficients owing to solid solution (especially of $MgCO_3$ in calcite), they may be mass-balanced with sufficient precision using conventional "end-member" formulae:

$$4 \text{ quartz} + 3 \text{ dolomite} + H_2O = \text{talc} + 3 \text{ calcite} + 3\ CO_2 \quad (1)$$

$$5 \text{ talc} + 4 \text{ quartz} + 6 \text{ calcite} = 3 \text{ tremolite} + 2\ H_2O + 6\ CO_2 \quad (2)$$

$$2 \text{ talc} + 3 \text{ calcite} = \text{tremolite} + \text{dolomite} + H_2O + CO_2 \quad (3)$$

$$\text{talc} + 4 \text{ quartz} + 2 \text{ dolomite} = \text{tremolite} + 4\ CO_2 \quad (4)$$

$$8 \text{ quartz} + 5 \text{ dolomite} + H_2O = \text{tremolite} + 3 \text{ calcite} + 7\ CO_2 \quad (5)$$

The isobaric invariant point in Figure 1 represents the intersection of a univariant P–T curve (five solid phases plus a fluid phase in the five-component system CMSH–CO_2) with the isobaric plane of the diagram. At a specified P, there can be no change in T nor in any of the chemical potentials. There must be a "closed-system" reaction that buffers the value of T with respect to any gain or loss of heat at constant mass of all components, and there must be a pair of "open-system" reactions that define and buffer the chemical potentials of H_2O and CO_2 with respect to any change in the number of moles of H_2O or CO_2.

The closed-system reaction

The reaction that takes place in response to a change in the heat content of the system at fixed mass of all components, thereby buffering T, must produce or consume H_2O–CO_2 fluid of isobarically invariant composition [$X(CO_2) = 0.48$]. It can be mass-balanced by conserving all five components among the five solid phases plus a fluid phase of invariant composition:

$$103 \text{ talc} + 156 \text{ calcite} = 51 \text{ tremolite} + 4 \text{ quartz} + 54 \text{ dolomite} + 100\ (H_2O)_{0.52}(CO_2)_{0.48} \quad (6)$$

This kind of reaction pertains not only to a closed system, but also to a type of open system commonly used in modeling prograde metamorphism, a system to which heat is added and volatile species escape at the same rate as they are being produced.

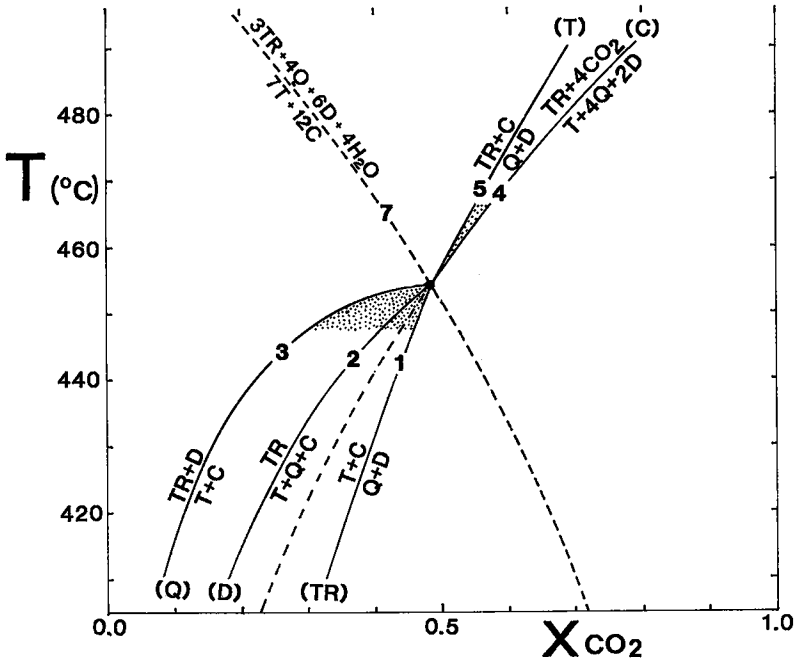

FIG. 1. T–$X(CO_2)$ diagram at P = 2 kbar. Isobarically univariant curves for Reactions 1 to 5 (see text), involving tremolite (TR), talc (T), quartz (Q), calcite (C) and dolomite (D), radiate from an isobaric invariant point at which all five phases are stable. The stipple pattern indicates the isobarically divariant stability fields of the reactant and product assemblages of Reaction 6, a "closed-system" reaction involving the five solid phases plus fluid of isobarically invariant composition. The dashed-line curves, representing Reaction 7 (a dehydration reaction that is metastable on both sides of the invariant point) and the metastable part of Reaction 4 (a decarbonation reaction), enable the invariant point to be located quickly and reliably by computer (see text). This and all subsequent phase diagrams have been computed using thermochemical data from Helgeson *et al.* (1978). H_2O fugacities are from Helgeson & Kirkham (1974); CO_2 fugacity coefficients are from C.W. Burnham and V.J. Wall (unpubl. written comm. 1974). Ideal mixing of H_2O and CO_2 is assumed. T-dependent activities of $CaCO_3$ and $MgCO_3$ in calcite coexisting with dolomite are given by Equations 10 and 3 of Skippen (1974); the thermochemical properties of dolomite are not explicitly involved in computing these curves.

Chemographic determination of reactants and products

Inspection of the phase-absent labels on the isobaric univariant curves in Figure 1 reveals a useful chemographic relationship. The absent phases on the low-T curves (tremolite, quartz, and dolomite) are the product phases of Reaction 6, and the absent phases on the high-T curves (talc and calcite) are the reactant phases. This relationship is valid for any isobarically invariant reaction in any mixed-volatile system.

Reactants and products also can be identified by inspection of the phase-present labeling. In Figure 1, the reactant assemblage of Reaction 6, *talc – calcite*, is seen to be limited by stable curves that span the largest divariant sector on the low-T side of the isobaric invariant point (Curves 1 and 3). Similarly, the product assemblage (*tremolite – quartz – dolomite*) is limited by curves that span the largest divariant sector on the high-T side of the point; in this special case, because only two curves emanate from the high-T side of the point, the "largest divariant sector" happens to be the only divariant sector. Bearing in mind that in systems with few components, a single isobaric curve may proxy for a "largest divariant sector", this relationship too is valid for any isobaric invariant point.

P–T projection.

If Figure 1 were projected parallel to its X coordinate onto a P–T diagram, the isobarically divariant stability fields of *talc - calcite* and of *tremolite - quartz - dolomite* would project as a pair of collinear isobaric lines that would meet end-to-end at the projection of the isobaric invariant point. Accordingly, on a polybaric P–T projection of a set of T–X diagrams, the stability fields of *talc - calcite* and of *tremolite - quartz - dolomite* project as a pair of divariant P–T fields separated by the polybaric trace of the isobaric invariant point. This exemplifies another completely general chemographic relationship.

In conclusion, it is appropriate to label the reactant and product assemblages on either side of the polybaric trace of any isobaric invariant point, thus revealing its kinship with other types of univariant P–T curve. For any closed-system, isobarically invariant reaction in any mixed-volatile system, the reactant and product assemblages may be identified by inspection of either the phase-absent or the phase-present labeling on the *complete* set of stable T–X curves that emanate from the isobaric invariant point. Alternatively, provided that the composition of the isobarically invariant fluid is known, there is no need to know the stable T–X topology; the reactant and product assemblages may be identified by algebraic mass-balancing of the closed-system reaction.

Let us now seek a convenient method of determining the composition of the isobarically invariant fluid.

The dehydration and decarbonation reactions

The reaction that buffers the chemical potential of H_2O with respect to a loss or gain of H_2O is a dehydration reaction

$$7 \text{ talc} + 12 \text{ calcite} = 3 \text{ tremolite} + 4 \text{ quartz} + 6 \text{ dolomite} + 4\ H_2O \qquad (7)$$

which involves all five solid phases, the coefficients of calcite and dolomite being such as to conserve CO_2. Although this reaction is stable only at the isobaric invariant point, its T–$X(CO_2)$ curve can be computed in the usual manner; it is plotted as a metastable (dashed) curve in Figure 1. The reaction that buffers the chemical potential of CO_2 is a decarbonation reaction. Because of compositional degeneracy, the coefficient for calcite happens to be zero, and therefore the reaction happens to be identical to Reaction 4, one of the stable isobaric univariant reactions.

For any isobarically invariant assemblage in any mixed-volatile system, there is an analogous pair of reactions, stable or metastable, each of which involves only one of the two volatile species (except in the special case where one of the stable T–X curves is an isothermal line representing a truly univariant reaction involving only solid phases). With rare exceptions, the isobaric T–X curves for the two reactions intersect at a high angle, and they have opposite slopes throughout the whole range of X (*e.g.*, see Fig. 1). This relationship provides a reliable and efficient algorithm to compute the isobarically invariant values of X and T at any specified value of P:

1. Mass-balance a reaction involving all the solid species and one of the two volatile species. (If there is compositional degeneracy, one or more of the solid species may have a coefficient of zero.)
2. Mass-balance a reaction involving all the solid species and the other volatile species.
3. At specified P, compute the equilibrium values of T at any two values of X for each of the two reactions, thus locating a pair of points on each T–X curve.
4. Compute an equation for a straight line through each of the two pairs of equilibrium points.
5. Compute the X value of the point of intersection of the two straight lines, defaulting to $X = 0.001$ or 0.999 if the point of intersection is respectively below or above that range.
6. Compute the equilibrium values of T for both reactions at the intersection-point value of X.
7. Test for convergence of the two values of T to some acceptable tolerance; either terminate or proceed.
8. Substitute the new values of X and T on each curve for the most remote of the initial values.
9. Return to Step 4.

To delineate mixed-volatile P–T curves, a computer program CARBOGRAD has been written in APL. Following execution of the foregoing algorithm, the coefficients of the two reactions are linearly combined in proportion to the equilibrium value of $X(CO_2)$, and each phase is identified as a reactant or product by its negative or positive coefficient, respectively. The whole procedure is then repeated at successively higher values of P so as to delineate the univariant P–T curve.

P–T Curves and Singular Points

Figure 2 is a P–T diagram on which the univariant curve for Reaction 6 has been plotted and labeled. The equilibrium value of $X(CO_2)$ increases from 0.28 at P = 5 kbar to 0.66 at P = 0.5 kbar, and the coefficients of Reaction 6 vary accordingly with changing P. As P decreases through 1.9 kbar, the coefficient of quartz changes

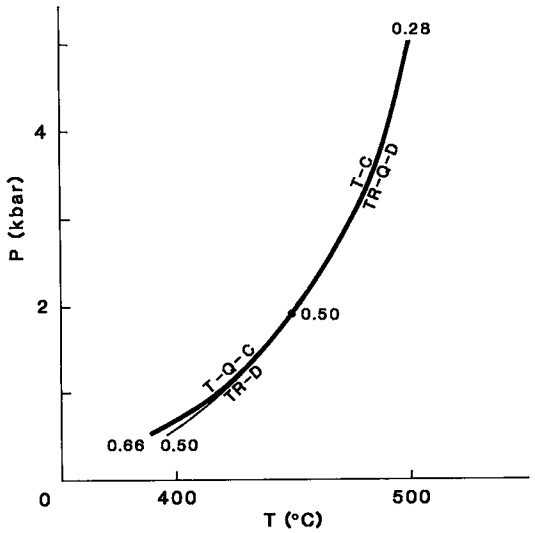

FIG. 2. P–T trace of the isobaric invariant point in Figs. 1 and 3 (bold line), labeled with the reactant and product assemblages of Reaction 6. A singular point indicates the P and T below which quartz becomes a reactant rather than a product. $X(CO_2)$ varies smoothly between the labeled values. The stable part of the P–T projection of the T-maximum for Reaction 3 (narrow line) terminates at the singular point, where it is tangential to the bold curve.

from positive (product) to negative (reactant). This generates a *singular point* on the curve, at which quartz has a coefficient of zero. At this point, the truly univariant reaction happens to be identical to Reaction 3, whose isobaric univariant curve passes through a T-maximum at $X(CO_2) = 0.5$. This relationship is illustrated in Figure 3, in which the polybaric trace of the univariant curve is displayed on T–$X(CO_2)$ coordinates. Note that the chemographic methods of determining reactant and product assemblages are valid on both sides of the singular point.

The T-maximum in the P–T–$X(CO_2)$ surface for Reaction 3 is stable only on the low-T side of the singular point, and projects as a univariant curve on the P–T plane (Fig. 2). A similar curve emanates tangentially from any such singular point toward either higher or lower P. As pointed out by Skippen (1974) and demonstrated in the field by Rice (1977a), an isograd based on such a curve would be rigorously constrainable only from the low-T side. Such curves will not be discussed further, nor will they be plotted on subsequent P–T diagrams.

In general, a P–T singular point is present wherever an isobaric invariant point happens to coincide with a T maximum on any of the stable isobaric univariant curves passing through that point. On a univariant curve that spans a wide range of $X(CO_2)$ values with changing P, there may be several singular points. Any singular point may be located directly, by algebraic mass-balancing of the closed-system reaction at different values of P; there is no need to mass-balance the set of isobarically univariant reactions nor to work out their stable T–$X(CO_2)$ topology.

Although singular points have invariant P–T coordinates, they are not of any use for thermobarometry, because there is nothing distinctive about the phases or phase assemblages at higher and lower values of P along the univariant curve.

P–T DIAGRAM

The foregoing considerations facilitate direct chemographic mapping of the stable univariant P–T curves corresponding to the isobaric invariant points on any T–X diagram. For part of the system CMSH–CO_2, such a mapping has been done, using the CARBOGRAD program in an interactive manner. Each P–T curve is traced until it meets another curve that restricts its stability, thus locating a P–T invariant point. Then, for each additional stable univariant curve emanating from the invariant point, the appropriate pair of dehydration and decarbonation reactions is balanced, and the stable part of its P–T curve is mapped. The resulting P–T diagram (Fig. 4) has 28 univariant curves and 5 mixed-volatile invariant points. There is also one invariant point in the CO_2-free subsystem (the point near 9 kbar, 800°C). With changing P or T along the univariant curve through each of the 13 singular points, one of the reactant phases becomes a product phase or *vice versa*, as a consequence of the changing composition of the isobarically invariant fluid.

From the $X(CO_2)$ values labeled on each of the P–T curves and points in Figure 4, it can be seen that without exception, $X(CO_2)$ decreases with increasing P along each curve. Considering that each curve may be regarded as the line of intersection of a P–T–X equilibrium surface for a decarbonation reaction with that for a dehydration reaction, this decrease may be regarded as due to the fact that P–T curves for decarbonation reactions generally have a modest positive slope, whereas those for dehydration reactions generally steepen and slope negatively with increasing P.

As a result of the singular points, P–T diagrams such as that in Figure 4 may appear to be inconsistent with established chemographic rules. For example, two curves that limit the stability of *enstatite* + *tremolite* intersect near 7.5 kbar, 640°C, but are stable on both sides of their point of intersection. This is chemographically permis-

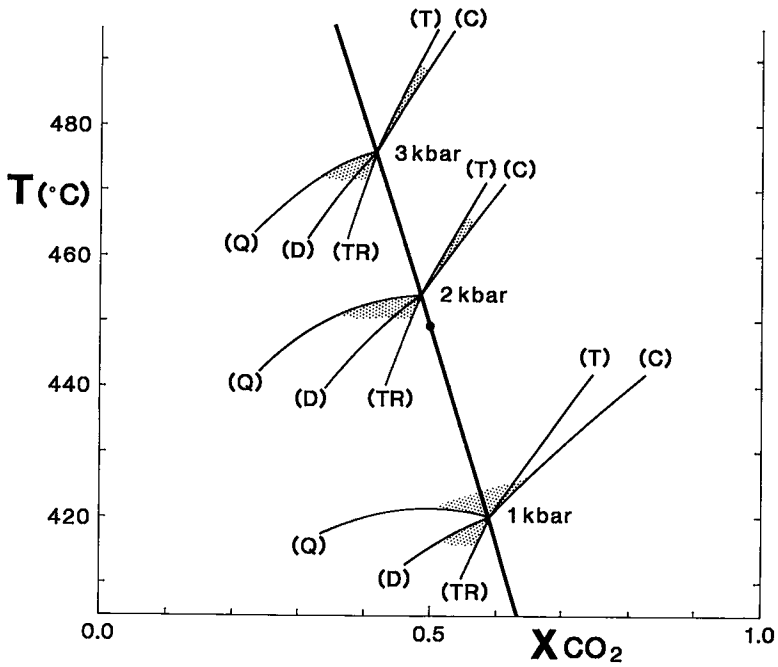

FIG. 3. Polybaric T–$X(CO_2)$ projection of part of the univariant P–T curve in Fig. 2 (bold line), including the singular point. Also shown are isobaric contours on the P–T–X surfaces for Reactions 1 to 5 at 1, 2, and 3 kbar. The stipple pattern indicates the isobarically divariant stability fields of the reactant (lower-T) and product (higher-T) assemblages for the isobarically invariant Reaction 6. Both above and below the singular point, note that the reactant phases are absent on the high-T curves, and the product phases are absent on the low-T curves. This chemographic relationship is valid for any isobarically invariant reaction in any mixed-volatile system.

sible because the two curves are at different values of $X(CO_2)$. On a T–$X(CO_2)$ diagram, the isobaric invariant points corresponding to any such pair of curves are at opposite ends of a stable T–$X(CO_2)$ curve having a thermal maximum. A reactant assemblage can have only one upper limit of P–T stability, but a product assemblage may have more than one lower limit of P–T stability at different values of $X(CO_2)$. Wherever any two P–T curves meet *at the same value of* $X(CO_2)$, the method of Schreinemakers may be applied in the usual way.

Figure 4 may be simplified by stipulating that one or more of the solid phases be present in excess. For example, a stipulation that all assemblages include calcite eliminates all the calcite-absent curves and obviates the need to label calcite on the remaining curves. The resulting diagram (Fig. 5) displays all P–T constraints that pertain to mineral assemblages that include calcite, *i.e.*, virtually all siliceous dolomitic marbles. The calcite-present stipulation also eliminates a singular point at which the coefficient of calcite changes sign (Fig. 4, at about 2.3 kbar, 610°C). The chemographic relationship of Figure 5 to calcite-in-excess T–$X(CO_2)$ diagrams is exactly analogous to that of Figure 4 to fully expanded T–$X(CO_2)$ diagrams.

ISOGRADS BASED ON UNIVARIANT MIXED-VOLATILE REACTIONS

Armed with a reliable method of identifying the reactant and product assemblage for any univariant mixed-volatile reaction, it is now possible to investigate whether isograds based on this type of reaction may be rigorously mappable, using the pair of mineral assemblages or subassemblages that are *necessary and sufficient* to constrain the isograd from both sides, in the manner previously advocated for isograds in metapelites (Carmichael 1970, p. 148–152).

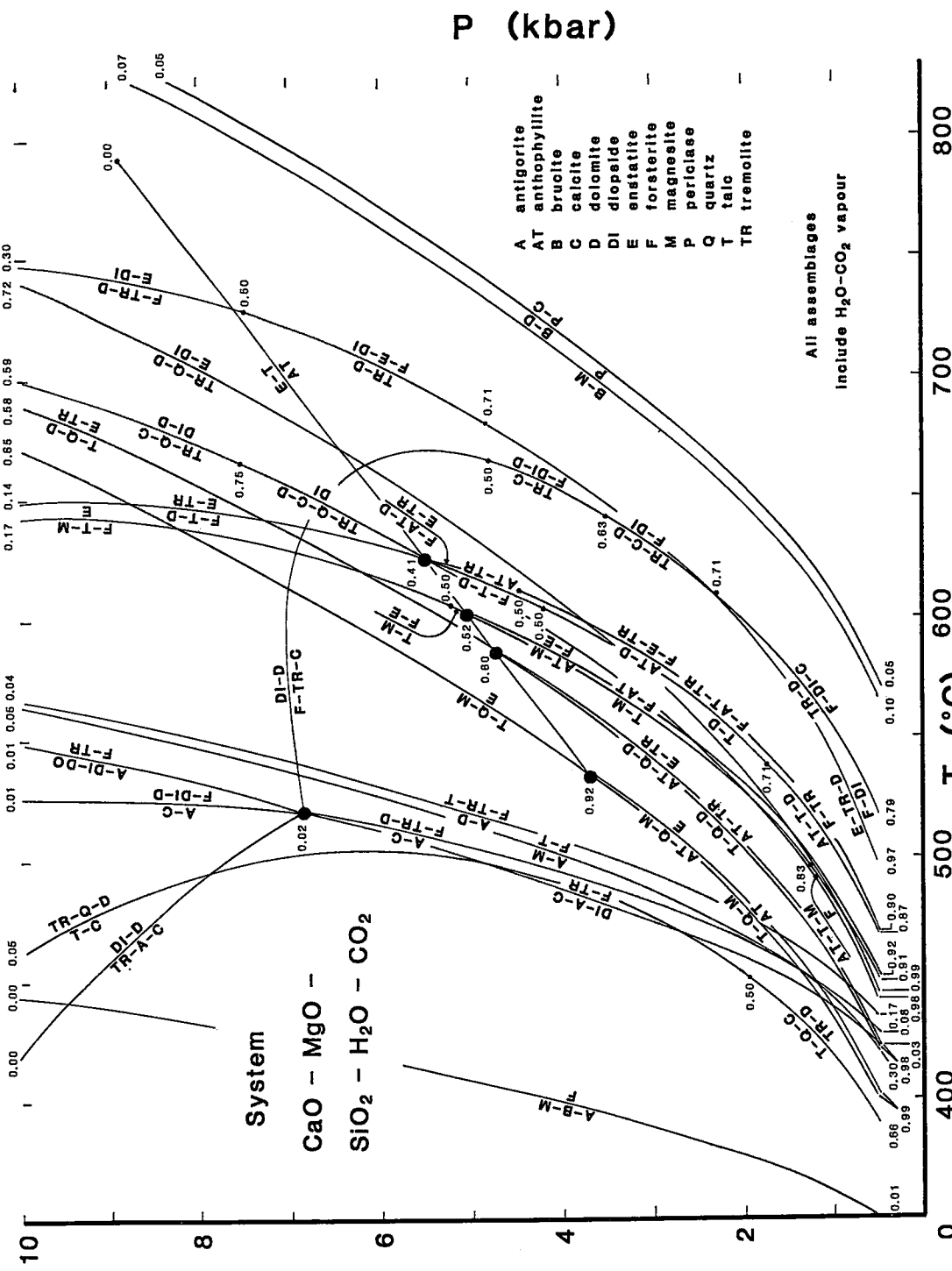

FIG. 4. P–T phase diagram for some reactions in the mixed-volatile-fluid-present part of the system CMSH–CO_2. Large dots are invariant points, and small dots are singular points (see text). $X(CO_2)$ varies smoothly between the values labeled on each curve and point.

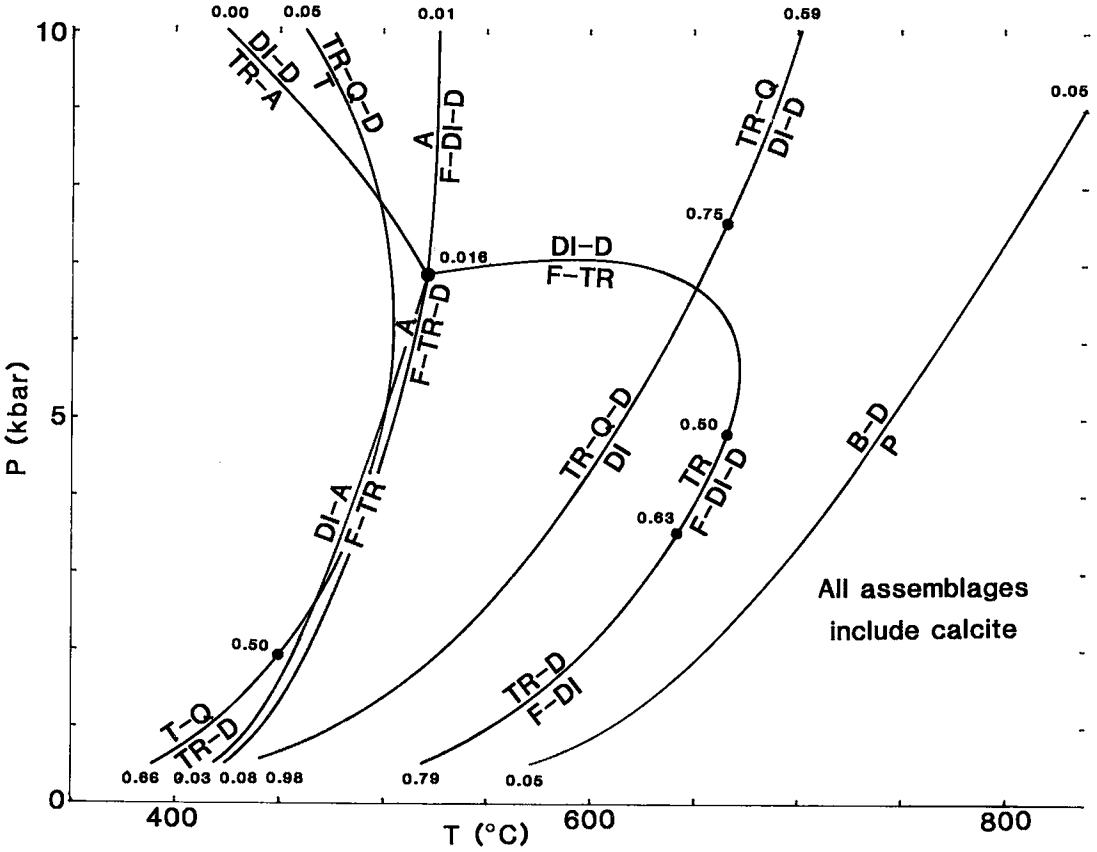

FIG. 5. P–T phase diagram, simplified from Fig. 4 by the stipulation that calcite is present in excess.

Contact aureole of the Kaizuki-yama granite, Japan

In Paleozoic siliceous dolomitic marble intruded by a Cretaceous granitic pluton, Suzuki (1977) delineated zone boundaries that coincide with occurrences of the assemblages *tremolite – talc – quartz – calcite – dolomite*, *diopside – tremolite – quartz – calcite – dolomite*, and *forsterite – diopside – tremolite – calcite – dolomite*. Each of these assemblages corresponds to a univariant curve in Figure 4 (or Fig. 5, since each includes calcite). Suzuki's map of the areal distribution of mineral assemblages in his contact aureole (his Fig. 1, p. 82) can be used in conjunction with Figure 4 (or 5), as a test of whether his zone boundaries can be mapped as reaction isograds.

Suzuki's calcite–dolomite temperatures for his three zone boundaries (465°C, 555°C, and 595°C), taken in conjunction with the corresponding curves in Figure 4 or 5, indicate apparent pressures of 2.5, 2.8, and 1.9 kbar for the three zone boundaries. Assuming a uniform pressure of about 2.5 kbar across the contact aureole, one can see from Figure 4 or 5 that the three potentially mappable isograds are based on Reaction 6 and on the following two reactions:

$$\text{tremolite} + \text{quartz} + \text{calcite} + \text{dolomite} = \text{diopside} + \text{fluid} \quad (8)$$

$$\text{tremolite} + \text{calcite} + \text{dolomite} = \text{forsterite} + \text{diopside} + \text{fluid} \quad (9)$$

The tremolite – quartz – dolomite isograd. In Figure 6A, all occurrences of *tremolite – quartz – dolomite* and of *talc – calcite* from the western part of Suzuki's map have been plotted, so as to delineate an isograd based on Reaction 6. That the five-phase assemblage has no "zone of persistence" (Carmichael 1979, Ridley & Thompson 1986) is consistent with Suzuki's microprobe evidence that

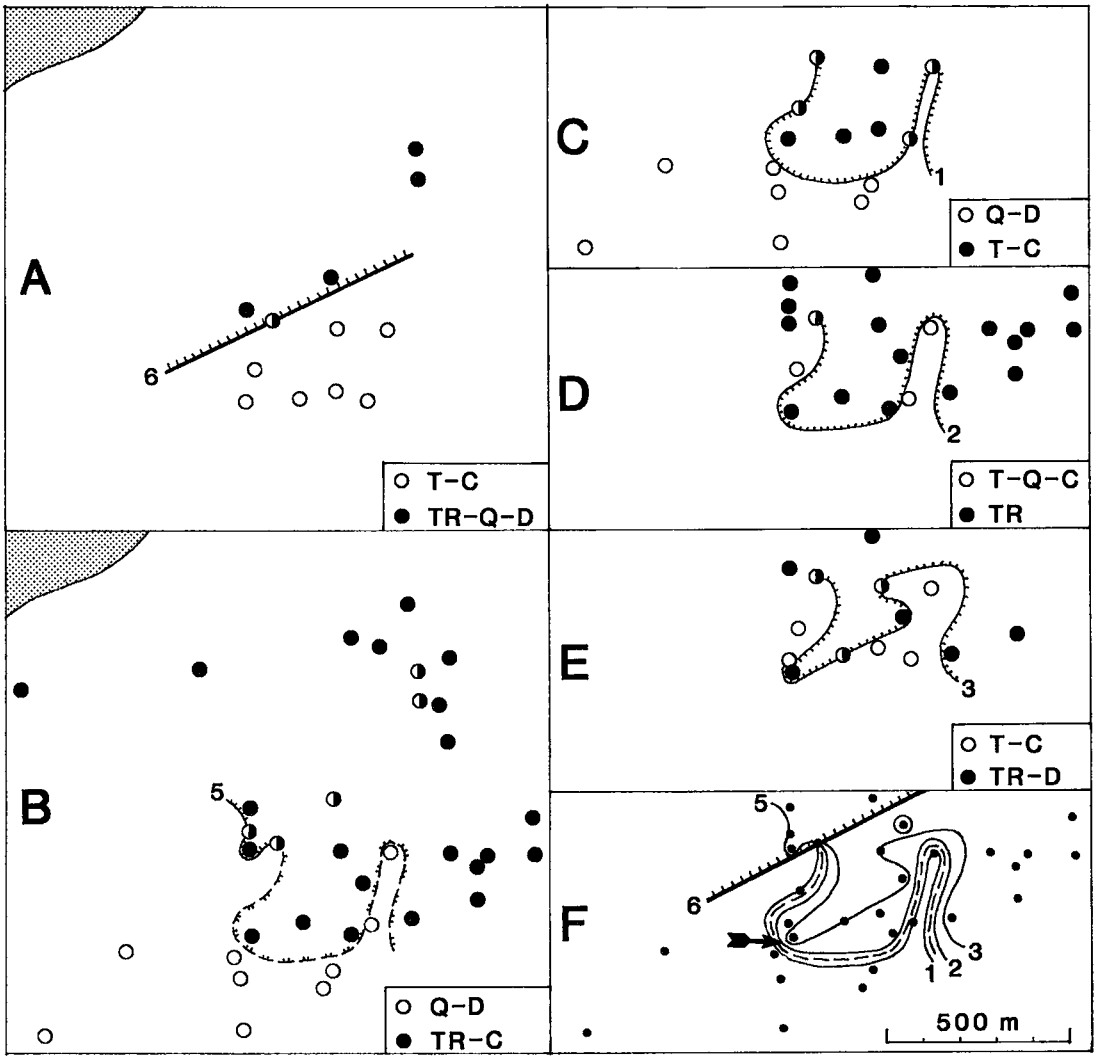

FIG. 6. Reaction isograds in part of the contact aureole of the Kasuga-mura granite (stipple pattern), central Honshu, Japan, constrained by assemblages or subassemblages of reactant and product minerals from Suzuki (1977, Fig. 1, p. 82). A: Tremolite – quartz – dolomite isograd, based on Reaction 6, with hachures on the higher-T side. This isograd is permissively coincident with Suzuki's Zone 2/1 boundary. B, C, D, E: Isograds based on Reactions 5, 1, 2, and 3, respectively, with hachures on the higher-T or lower-$X(CO_2)$ side (or both; see Fig. 1). Apparently, these isograds delineate a lobate "front" of infiltration of H_2O-rich fluid toward the south-southwest. F: Synoptic map showing all sample localities (dots) and all five isograds. The arrow indicates where the infiltration front is most tightly constrained by samples (see text). The circled locality, an occurrence of the assemblage *diopside – quartz – calcite* (see Fig. 7 and discussion in text), is another indication of pervasive local infiltration of H_2O-rich fluid.

the CMSH–CO_2 system provides a good approximation to its natural counterpart, and supports the inference that equilibrium was closely approached, in the presence of an H_2O–CO_2 fluid phase, at the thin-section scale. That the isograd is permissively parallel to the contact of the granite pluton is consistent with its theoretical independence of any variation in $X(CO_2)$. The isograd also is permissively coincident with Suzuki's zone boundary. Thus, the boundary between Suzuki's Zones 1 and 2 is seen to be a well-behaved reaction isograd, which may be named unambiguously in

accord with its complete product-assemblage: the *tremolite – quartz – dolomite isograd* (*cf.* Carmichael 1970).

Note that if the pair of "critical assemblages" listed by Skippen (1974, Table 3, p. 507) were used for "bracketting this point in the field" (*talc – quartz – calcite – dolomite* and *tremolite – quartz – calcite – dolomite*), four of the seven constraining samples in the lower-grade zone would be eliminated because they lack quartz. Skippen's critical assemblages are unduly restrictive, because at a pressure greater than 1.9 kbar, neither quartz nor dolomite is a necessary part of the lower-grade critical assemblage. Similarly, calcite need not be present in the higher-grade critical assemblage. Note, however, that calcite *is* present in all of Suzuki's samples. Absence of calcite in this assemblage would imply a bulk-rock (Mg + Fe + Mn)/Ca atomic ratio greater than unity, *i.e.*, more magnesian than normal siliceous dolomitic marble.

Variation of $X(CO_2)$: buffering versus infiltration. Buffering and infiltration are widely regarded as independent phenomena, and there has been much discussion as to how to distinguish their effects on metamorphic and metasomatic rocks. In a review of many such studies, Rice & Ferry (1982, p. 304) appealed for modal analyses in all studies of buffering phenomena concluding that "only from modes can buffering with infiltration be rigorously distinguished from buffering without infiltration." Further, they concluded that Suzuki's study of the Kaizuki-yama contact aureole is one of a large group of studies in which fluid composition appears to have been controlled by "buffering alone without evidence for infiltration" (*ibid.*, p. 301). These conclusions may be tested by using Suzuki's mineral-assemblage data to map isograds based on isobarically univariant reactions, *i.e.*, isograds whose configuration depends on $X(CO_2)$ as well as T.

In Figure 6B, C, D, and E respectively, isograds based on Reactions 5, 1, 2, and 3 have been constrained and delineated, and all five isograds are compiled in Figure 6F. Note that the topological relationship among these isograds is identical to that among the isobaric univariant curves in Figure 1; this is a condition that must be met by any properly mapped set of reaction isograds. In particular, note that the tremolite–calcite isograd (Fig. 6B) is tightly constrainable even where it is metastable with respect to the pair of isograds based on Reactions 1 and 2.

Assuming that the isotherms were parallel to the granite contact and that the initial assemblage in all samples was *quartz – calcite – dolomite*, these isograds appear to outline an irregular zone that was infiltrated toward the south-southwest by H_2O-rich fluid. The postulated infiltration "front" is most abrupt at the locality indicated by the arrow in Figure 6F, where all three of the lower-T isograds are seen to be bracketed between a *quartz – dolomite (– calcite)* specimen and a *tremolite – dolomite (– calcite)* specimen only 70 m to the northeast. Suzuki's calcite-dolomite temperature for this locality is ~430°C. Assuming equilibrium at 2.5 kbar, this would imply that $X(CO_2)$ is greater or equal to 0.35 for the southwestern specimen and less than or equal to 0.1 for the northeastern specimen, so as to completely span the $X(CO_2)$ range of stability of talc–calcite (see Fig. 1). Assuming that both specimens were initially quartz–calcite–dolomite rocks, it is evident that *local* infiltration of H_2O-rich fluid completely overwhelmed the $X(CO_2)$-buffering capacity of the northeastern specimen (and three others; see Fig. 6E) in respect to Reactions 1, 2, and 3, whereas the southwestern specimen (and six others; see Fig. 6C) were unaffected. Only five of the 25 specimens in the talc–calcite zone contain isobarically univariant assemblages; the others are isobarically divariant. The configuration of the $X(CO_2)$-sensitive isograds provides evidence for pervasive *local* infiltration of H_2O-rich fluid. Hence we may conclude, even in the absence of modal data and contrary to the judgment of Rice & Ferry (1982), that prograde buffering of $X(CO_2)$ was only locally effective and was definitely accompanied by infiltration, at least in the outermost zone of this contact aureole. Nevertheless, the tremolite–quartz–dolomite isograd (Fig. 6A) is tightly constrainable. Evidently, mapping of this type of isograd can filter out not only regular effects of variation in $X(CO_2)$ (characteristic of prograde buffering) but also irregular effects (characteristic of *locally* pervasive infiltration).

The diopside isograd. In Figure 7, all occurrences of *tremolite – quartz – calcite – dolomite* and of *diopside* have been plotted, so as to delineate an isograd based on Reaction 8. Again, the isograd is permissively parallel to the contact of the granite and permissively coincident with Suzuki's corresponding zone-boundary. However, note that one occurrence of diopside (with quartz and calcite) is more than 300 m below the diopside isograd. Figure 4 or 5 shows that the diopside isograd based on Reaction 8 is constrainable only where $X(CO_2)$ is relatively high, and that diopside may occur at indefinitely lower T at low values of $X(CO_2)$. The configuration of the isograds in Figure 6F provides independent evidence that this specimen lies in a domain of relatively low $X(CO_2)$. Accordingly, this occurrence is inferred to reflect local infiltration of sufficient H_2O-rich fluid to overwhelm the buffer-

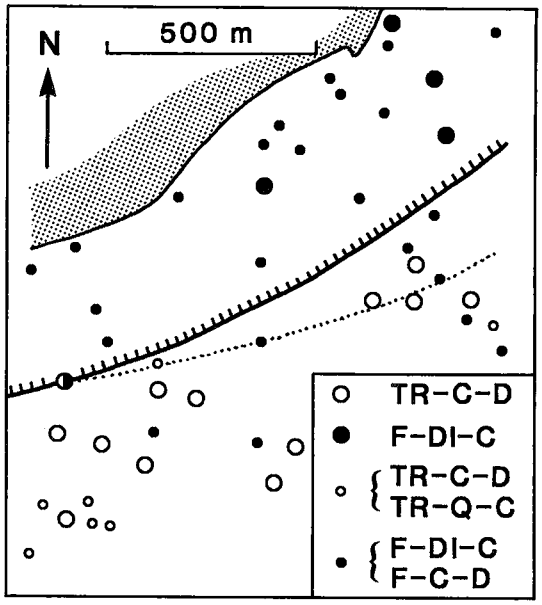

FIG. 7. Diopside isograd in the same part of Suzuki's contact aureole as in Fig. 6, based on Reaction 8. The isograd, tightly constrainable only if and where the fluid phase is rich in CO_2, is permissively coincident with Suzuki's Zone 3/2 boundary. The most southerly solid circle, an occurrence of *diopside - quartz - calcite*, is attributed to local infiltration of H_2O-rich fluid (see Fig. 6 and discussion in text).

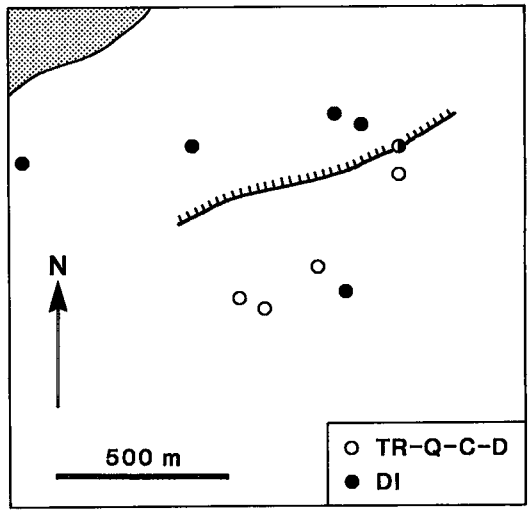

FIG. 8. Forsterite - diopside - calcite isograd in the eastern part of Suzuki's contact aureole, based on Reaction 9. Two occurrences of the reactant subassemblage *tremolite - calcite - dolomite* (large open circles) cause the isograd to diverge from Suzuki's Zone 4/3 boundary (dotted line).

ing capacity of the isobarically univariant reaction tremolite + 2 quartz + 3 calcite = 5 diopside + H_2O + CO_2 (10). Suzuki's calcite-dolomite temperature for this vicinity is ~455°C. Assuming equilibrium at 2.5 kbar, the infiltrating fluid must have had $X(CO_2)$ not greater than ~0.1, in order for diopside to be more stable than tremolite in the presence of quartz and calcite.

This "anomalous" occurrence of diopside illustrates the fact that for any univariant mixed-volatile reaction that does not impose a unique lower-T limit on its product assemblage, there is an upper limit to the range of variation in $X(CO_2)$ that can be filtered out. When mapping the corresponding isograd, one must bear in mind the possibility that if the variation of $X(CO_2)$ exceeds that range, there may be anomalous occurrences of the product assemblage.

The forsterite - diopside - calcite isograd. In Figure 8, an isograd based on Reaction 9 has been delineated, using occurrences of the subassemblages *tremolite - calcite - dolomite* and *forsterite - diopside - calcite* from the eastern part of Suzuki's Figure 1. Calcite is stipulated as part of both subassemblages to allow for the possibility that calcite may be either a reactant or a product, depending on whether the pressure is greater or less than that of the singular point at 2.3 kbar on the corresponding P-T curve (see Fig. 4). Note that, in this case, there are two constraining samples that force the isograd to diverge from Suzuki's zone boundary and to be more nearly parallel to the contact of the granite.

Because the small solid dots in Figure 8 represent occurrences of either *forsterite - diopside - calcite* or *forsterite - calcite - dolomite*, they may or may not constrain the isograd from the high-grade side. Similarly, because the small open circles represent occurrences of either *tremolite - calcite - dolomite* or *forsterite - calcite - dolomite*, they may or may not constrain the isograd from the low-grade side. Evidently, Suzuki's use of one symbol to represent occurrences of more than one mineral assemblage has obliterated some of the valid constraints on this isograd. The same may be said of Isograd I of Rice (1977a, Fig. 2, p. 4). Because in most cases it is neither practical nor worthwhile to publish maps with a unique symbol for every unique mineral assemblage, it is all the more important to identify critical subassemblages and to make full use of them in mapping reaction isograds. For this purpose, Figures 4 and 5 should be a useful tool.

Bathograds Based on Invariant Mixed-Volatile Reactions

Four of the five mixed-volatile invariant points in Figure 4 lie on a highly degenerate P–T curve for a volatile-conservative reaction,

4 enstatite + talc = anthophyllite (11)

Because the change of volume in Reaction 11 is only +1%, these four invariant points are not suitable for barometric purposes (*cf.* Evans & Trommsdorff 1974). The fifth invariant point imposes a lower limit of pressure on the assemblage or subassemblage *diopside – antigorite – dolomite*. The fluid-conservative reaction at this point is

259 diopside + 2 antigorite + 135 dolomite = 90 forsterite + 62 tremolite + 270 calcite (12)

This reaction also has a relatively small ΔV (+5%); the invariant point is therefore sensitive both to uncertainties in the thermochemical data and to partitioning of additional components. Nevertheless, it shows promise as a much-needed barometric indicator within the greenschist facies of regional metamorphism.

Figure 4 is computed from the data-base of Helgeson *et al.* (1978), assuming ideal mixing of H_2O and CO_2, and using $CaCO_3$ and $MgCO_3$ in calcite coexisting with dolomite as reacting species, as described by Skippen (1974). Using dolomite at unit activity rather than $MgCO_3$ in calcite, the invariant point is at 5.5 kbar, 505°C. Using UBCDATA (Berman *et al.* 1985, Berman 1988) and GEØ-CALC software (Brown *et al.* 1988), which incorporates the H_2O–CO_2 mixing model of Kerrick & Jacobs (1981), the invariant point is at 6.2 kbar, 535°C. For typical compositions of coexisting minerals in Alpine rocks (Trommsdorff & Evans 1972, 1977a), assuming ideal mixing in the octahedrally coordinated sites of all minerals, the invariant point is displaced about +1.1 kbar and +2°C. In the presence of graphite, owing to generation of significant concentrations of CH_4, H_2, and CO in the fluid phase, the invariant point is displaced about –0.3 kbar and –30°C (calculated with the equations of Ohmoto & Kerrick 1977).

To map a metamorphic bathograd based on this invariant point, occurrences of *diopside – antigorite – dolomite* and of the low-P assemblage or subassemblage *forsterite – tremolite – calcite* should be plotted on a regional-scale map, and the most regular surface that would separate all such occurrences should be traced on the topographic surface. The resulting bathograd would be within the P-range of Bathozone 5, whose upper and lower P-limits are defined, respectively, by the metapelitic subassemblages *garnet – kyanite – biotite* and *sillimanite – muscovite – plagioclase – quartz* (Carmichael 1978).

In the Swiss and Italian Alps, north and east of the Bergell intrusive complex, *diopside – antigorite – dolomite* occurs regionally in greenschist-facies metaperidotite, ophicarbonate, and siliceous marble (Skippen & Trommsdorff 1975). In the Bergell contact aureole, by contrast, *forsterite – tremolite – calcite* occurs in association with metapelitic assemblages diagnostic of Bathozones 1 and 2 (Trommsdorff & Evans 1977a, Carmichael 1978, Fig. 6, p. 788). Assuming equilibrium in the presence of a fluid phase, these data indicate that the low-grade rocks north and east of the Bergell Complex were metamorphosed at much higher pressure than the contact aureole. This conclusion is tenable only if the low-grade regional metamorphism is significantly older than the contact metamorphism. Thus, it is consistent with the geological synthesis of Trommsdorff & Nievergelt (1983), but contrary to that of Wenk (1973, 1982).

Discussion and Conclusions

A P–T diagram such as that in Figure 4 or 5, on which univariant curves for mixed-volatile reactions have been plotted and labeled, is a convenient tool for abstracting all possible P–T information from silicate–carbonate mineral-assemblage data. Variation in $X(CO_2)$ has no effect on the position of the P–T curves, but some $X(CO_2)$ information can be retained if $X(CO_2)$ values are labeled on the curves. Such a phase diagram identifies low-variance mineral assemblages, for which P–T estimates may be refined through microprobe analysis of the coexisting minerals, and critical subassemblages that are necessary and sufficient for rigorous mapping of mixed-volatile reaction isograds and bathograds whose configuration is independent of variation in $X(CO_2)$. The system CaO–MgO–SiO_2–H_2O–CO_2 features one invariant point that shows promise as a much-needed barometric indicator in the greenschist facies of regional metamorphism. We may anticipate that P–T diagrams for other mixed-volatile systems will feature many more invariant points, at least some of which should provide new tools for quantitative thermobarometry, and a basis for extending the mapping of metamorphic bathozones beyond the amphibolite-facies terranes to which they are currently restricted.

Acknowledgements

Hugh Greenwood's 1962 paper changed the

course of my career. Here was the explanation for my intersecting isograds (Carmichael 1967, 1970), published three years before I had even mapped them! Here was a branch of geology with theoretical rigor and powerful predictive capability. All my measurements of deformed pebbles were carefully filed away, and I have been enjoying the study of metamorphism ever since. Stimulating discussions with Greenwood and with George B. Skippen helped to clarify my thinking on low-variance phase equilibria. A preliminary version of this paper was presented at the Geological Association of Canada - Mineralogical Association of Canada Annual Meeting in Ottawa (Carmichael 1986). The final version has benefitted from perceptive reviews by David A. Hewitt and Jack M. Rice. My research program is supported by an operating grant from the Natural Sciences and Engineering Research Council.

REFERENCES

BAKER, J., HOLLAND, T. & POWELL, R. (1991): Isograds in internally buffered systems without solid solutions: principles and examples. *Contrib. Mineral. Petrol.* **106,** 170-182.

BERMAN, R.G. (1988): Internally consistent thermodynamic data for minerals in the system Na_2O - K_2O - CaO - MgO - FeO - Fe_2O_3 - Al_2O_3 - SiO_2 - TiO_2 - H_2O - CO_2. *J. Petrol.* **29**, 445-522.

_____, BROWN, T.H. & GREENWOOD, H.J. (1985): An internally consistent thermodynamic data base for minerals in the system Na_2O - K_2O - CaO - MgO - FeO - Fe_2O_3 - Al_2O_3 - SiO_2 - TiO_2 - H_2O - CO_2. *Atomic Energy Can. Ltd., Tech. Rep.* **377**.

BROWN, T.H., BERMAN, R.G. & PERKINS, E.H. (1988): GEØ-CALC: software package for calculation and display of pressure - temperature - composition phase diagrams using an IBM or compatible personal computer. *Comput. & Geosci.* **14**, 279-289.

CARMICHAEL, D.M. (1967): *Structure and Progressive Metamorphism in the Whetstone Lake Area, Ontario.* Ph.D. dissertation, Univ. California, Berkeley, California.

_____ (1970): Intersecting isograds in the Whetstone Lake Area, Ontario. *J. Petrol.* **11**, 147-181.

_____ (1978): Metamorphic bathozones and bathograds: a measure of the depth of post-metamorphic uplift and erosion on the regional scale. *Am. J. Sci.* **278**, 769-797.

_____ (1979): Some implications of metamorphic reaction mechanisms for geothermobarometry based on solid-solution equilibria. *Geol. Soc. Am., Abstr. Programs* **11**, 398.

_____ (1986): Chemographic expansion of mixed-volatile equilibria in P-T space. *Geol. Assoc. Can. - Mineral. Assoc. Can., Program Abstr.* **11**, 52.

CONNOLLY, J.A.D. & TROMMSDORFF, V. (1991): Petrogenetic grids for metacarbonate rocks: pressure-temperature phase-diagram projection for mixed-volatile systems. *Contrib. Mineral. Petrol.* **108,** 93-105.

ELLIS, D.E. & WYLLIE, P.J. (1979): Carbonation, hydration, and melting relations in the system MgO-H_2O-CO_2 at pressures up to 100 kilobars. *Am. Mineral.* **64**, 32-40.

ERDMER, P. (1981): Metamorphism at the northwest contact of the Stanhope Pluton, Quebec Appalachians: mineral equilibria in interbedded pelite and calc-schist. *Contrib. Mineral. Petrol.* **76,** 109-115.

EUGSTER, H.P. & WONES, D.R. (1962): Stability relations of the ferruginous biotite, annite. *J. Petrol.* **3**, 82-125.

EVANS, B.W. & TROMMSDORFF, V. (1974): Stability of enstatite + talc, and CO_2-metasomatism of metaperidotite, Val d'Efra, Lepontine Alps. *Am. J. Sci.* **274**, 274-296.

FRANZ, G. & SPEAR, F.S. (1983): High pressure metamorphism of siliceous dolomites from the central Tauern Window. *Am. J. Sci.*, **283-A**, 396-413.

GREENWOOD, H.J. (1962): Metamorphic reactions involving two volatile components. *Carnegie Inst. Wash. Yearbook* **61**, 82-85.

_____ (1967): Mineral equilibria in the system MgO-SiO_2-H_2O-CO_2. *In* Research in Geochemistry **2** (P.H. Abelson, ed.). John Wiley & Sons, New York (542-567).

_____ (1975): Buffering of pore fluids by metamorphic reactions. *Am. J. Sci.* **275**, 573-593.

HELGESON, H.C., DELANY, J.M., NESBITT, H.W. & BIRD, D.K. (1978): Summary and critique of the thermodynamic properties of rock-forming minerals. *Am. J. Sci.* **278-A.**

_____ & KIRKHAM, D.H. (1974): Theoretical prediction of the thermodynamic behavior of aqueous electrolytes at high pressures and temperatures. I. Summary of the thermodynamic/electrostatic properties of the solvent. *Am. J. Sci.* **274**, 1089-1198.

KERRICK, D.M. & JACOBS, G.K. (1981): A modified

Redlich-Kwong equation for H_2O, CO_2, and H_2O-CO_2 mixtures at elevated pressures and temperatures. *Am. J. Sci.* **281**, 735-767.

OHMOTO, H. & KERRICK, D.M. (1977): Devolatilization equilibria in graphitic systems. *Am. J. Sci.* **277**, 1013-1044.

PUHAN, D. & HOFFER, E. (1973): Phase relations of talc and tremolite in metamorphic calcite–dolomite sediments in the southern portion of the Damara Belt (South West Africa). *Contrib. Mineral. Petrol.* **40**, 207-214.

RICE, J.M. (1977a): Progressive metamorphism of impure dolomitic limestone in the Marysville aureole, Montana. *Am. J. Sci.* **277**, 1-24.

_____ (1977b): Contact metamorphism of impure dolomitic limestone in the Boulder aureole, Montana. *Contrib. Mineral. Petrol.* **59**, 237-259.

_____ & FERRY, J.M. (1982): Buffering, infiltration, and control of intensive variables during metamorphism. *In* Characterization of Metamorphism through Mineral Equilibria (J.M. Ferry, ed.). *Rev. Mineral.* **10**, 263-326.

RIDLEY, J. & THOMPSON, A.B. (1986): The role of mineral kinetics in the development of metamorphic microtextures. *In* Fluid-Rock Interactions during Metamorphism (Advances in Physical Geochemistry **5**) (J.V. Walther & B.J. Wood, eds.). Springer-Verlag, New York (154-193).

SKIPPEN, G. (1974): An experimental model for low pressure metamorphism in siliceous dolomitic marble. *Am. J. Sci.* **274**, 487-509.

_____ & CARMICHAEL, D.M. (1977): Mixed-volatile equilibria. *In* Application of Thermodynamics to Petrology and Ore Deposits (H.J. Greenwood, ed.). *Mineral. Assoc. Can., Short Course Handbook* **2**, 109-125.

_____ & TROMMSDORFF, V. (1975): Invariant phase relations among minerals on T-X_{fluid} sections. *Am. J. Sci.* **275**, 561-572.

SUZUKI, K. (1977): Local equilibrium during the contact metamorphism of siliceous dolomites in Kasuga-mura, Gifu-ken, Japan. *Contrib. Mineral. Petrol.* **61**, 79-89.

THOMPSON, A.B. (1983): Fluid-absent metamorphism. *J. Geol. Soc. (London)* **140**, 533-547.

TROMMSDORFF, V. (1972): Change in T-X during metamorphism of siliceous dolomitic rocks of the Central Alps. *Schweiz. Mineral. Petrogr. Mitt.* **52**, 567-571.

_____ & EVANS, B.W. (1972): Progressive metamorphism of antigorite schist in the Bergell Tonalite aureole (Italy). *Am. J. Sci.* **272**, 423-437.

_____ & _____ (1977a): Antigorite-ophicarbonates: contact metamorphism in Valmalenco, Italy. *Contrib. Mineral. Petrol.* **62**, 301-312.

_____ & _____ (1977b): Antigorite-ophicarbonates: phase relations in a portion of the system CaO-MgO-SiO_2-H_2O-CO_2. *Contrib. Mineral. Petrol.* **60**, 39-56.

_____ & NIEVERGELT, P. (1983): The Bregaglia (Bergell) Iorio intrusive and its field relations. *Soc. Geol. Ital., Mem.* **26**, 55-68.

WENK, H.-R. (1973): The structure of the Bergell Alps. *Eclogae Geol. Helv.* **66**, 255-291.

_____ (1982): A geological history of the Bergell granite and related rocks. *In* Transformists Petrology. Theophrastus Publications, Athens.

WINKLER, H.G.F. (1974): *Petrogenesis of Metamorphic Rocks* (3rd edition). Springer-Verlag, New York.

Received September 12, 1988, revised manuscript accepted December 4, 1990.